Thai Journal of **Math**ematics
Volume 19 Number 3 (2021)
Pages 1037–1055

http://thaijmath.in.cmu.ac.th

ISSN 1686-0209

Study of Heat and Mass Transfer in MHD Flow of Sutterby Ferrofluid over a Curved Stretching Surface with Magnetic Dipole and Chemical Reaction Effect

Auwalu Hamisu Usman[1,2,3], **Noor Saeed Khan**[2,4], **Sadiya Ali Rano**[3], **Murtala Maitama**[5] **and Usa Wannasingha Humphries**[1*]

[1] *Department of Mathematics, Faculty of Science, King Mongkut's University of Technology Thonburi (KMUTT), 126 Pracha Uthit Road, Bang Mod,Thung Khru, Bangkok 10140, Thailand*
[2] *KMUTTFixed Point Research Laboratory, KMUTT-Fixed Point Theory and ApplicationsResearch Group, Faculty of Science, King Mongkuts University of Technology Thonburi (KMUTT),126 Pracha-Uthit Road, Bang Mod, Thrung Khru, Bangkok 10140, Thailand*
[3] *Department of Mathematical Sciences, Faculty of Physical Sciences, Bayero University, Kano. Kano, Nigeria*
[4] *Center of Excellence in Theoretical and Computational Science (TaCS-CoE), Science Laboratory Building, Faculty of Science, King Mongkuts University of Technology Thonburi (KMUTT), 126 Pracha-Uthit Road, Bang Mod, Thrung Khru, Bangkok 10140, Thailand*
[5] *Department of Mathematics, Federal Polytechnic, Kauran Namoda, Zamfara, Nigeria*
Email addresses: usa.wan@kmutt.ac.th (U. W. Humphries)

Abstract A study of non-Newtonian Sutterby ferrofluid and heat and mass transfer in the flow due to curved stretching sheets is presented.The flow in porous media is described using the Darcy-Forchheimer model which caused by the linear velocity of the curved stretching sheet. Concentration and energy equations are incorporated in the study of mass and heat transfer impacts. The motile microorganism equation included governing the swimming of the gyrotactic microorganism. The governing equations are transformed from nonlinear partial differential equation to ordinary differential equation and the solved using Homotopy Analysis method. The velocity is reduced due to dipole and non-Newtonian parameters effects. Temperature increases with the magnetic dipole and thermal radiation parameters. Concentration decreases with an increase in chemical reaction parameter and the concentration of microorganisms decreases with the Lewis number and increase with Peclet number. The numerical values of Nusselt, Sherwood and Local density numbers are presented in the tables.

MSC: 37N30; 34A08; 54H25
Keywords: Chemical reactions; Curved surface; Heat transfer; Magnetic dipole; Porosity media; Sutterby ferrofluid

Submission date: 27.04.2021 / Acceptance date: 29.06.2021

*Corresponding author.

Published by The Mathematical Association of Thailand.

1. Introduction

The law of Newton's viscosity does not apply to non-Newtonian fluids. The viscosity of a non-Newtonian fluid depends hugely on shear pressure and time for the perfect method. Several fundamental equations are developed due to the heterogeneity of non-Newtonian fluids. A growing interest in the biotechnology era has been investigated recently as a result of industrial and technological applications. Viscoelastic fluid is a non-Newtonian fluid with both viscous and elastic deformation properties. One type of fluid that accurately depicts the properties of viscoelastic fluid and diluted polymer solutions is Sutterby fluid Sutterby [1, 2]. The Sutterby fluid model is specifically equivalent to shear dilution and shear thickening in the case of high aqueous polymer solutions such as methylcellulose, hydroxyethyl cellulose, and carboxymethylcellulose Batra and Eissa [3]. Some studies on Sutterby fluids can be found in the references [4–6].

Due to the extreme wide range of practical applications in industry, such as porous insulation, geothermal systems, packages, waste disposal, crude oil extraction, food storage, oil technologies and fossil fuels, and so on, scientists are often very engaged in the flow of porous media. Various models have been developed in the literature, including Darcy and Brinkman and Darcy Forchheimer [7, 8]. Researchers are now interested in porous media models according to Darcy's law, s a result, numerous models are being developed. Kishan and Maripala [9] reported on the thermophoresis analysis and viscous dissipation effects on the mixed convection Darcy-Forchheimer MHD in a fluid saturated porous media. Rauf et al. [10] investigated on thermal radiation viscous fluid flow in Darcy-Forchheimer porous space over a curved moving surface. Jagadha and Amrutha [11] studied the Darcy-Forchheimer mixed convection MHD boundary layer flow with viscous dissipation in nanofluid saturated porous media.

Ferrofluids are a type of magnetized fluid that has had a significant technological impact and is currently being studied. Ferrofluid is a colloidal suspension of a single magnetic particle domain that is spread across a container and has a typical size of about 10 nm. Many industrial applications are commonly used, including nuclear aerodynamics, avionics, laser, robotics, fiber optics, cooling agents, semiconductor processing, crystal processing, cooling, filtration, plastic drawing, and computer peripherals. This prompted an increase in ferrofluid research by a number of researchers and scientists. The visual effects of magnetic dipoles on ferrofluide have been investigated by Anderson and Valnes [12]. Hayat [13] investigated on the exploration of the contribution of magnetic dipoles to the radiative flow of ferromagnetic Williamson fluid. References [14–16] show some important work on ferrofluid.

The Curve surface flow is a popular topic due to its indispensible applications in the polymer sector, engineering processes, and modern technology. Melt-spinning, extrusion of polymers from dying material, cooling of large metal plates in the bath, i.e. electrolytes, production of rubber and plastic sheets, wire drawing, paper manufacturing, polymer sheeting, thinning, glass fibers, filaments, winding rolls, liquid crystals in the condensation process, and so on are examples. The final quantity of a substance depends on the process of cooling and incarceration. Sakiadis [19] was the first to present a flow study due to the curved moving surface. Muhammad et al. [20] presented study on full developed Darcy-Forchheimer mixed convection flow via a curved surface. Ahmad et al. [21] studied a boundary layer flow over a curved surface embedded in porous media. Recent Khan et al. [22] investigated on the mathematical analysis of thermally radiative time dependent Sisko nanofluid flow on curved surface.

The current study focused on the Darcy-Forchheimer of hydromagnetic Sutterby ferromagnetic fluid flow over a curved stretching surface with the influence of chemical reaction, magnetic dipole and viscous dissipation. Partial differential equations are transformed into ordinary differential equations using an appropriate similarity transformation process and solved using the well-known homotopy analysis method HAM Liao [23–25]. However, many researchers [26–29] used HAM to solve their problems. The obtained results have been used to graphically discuss the effects of all related fluid parameters on all dimensionless profiles.

2. Mathematical Formulations

The 2-dimensional incompressible hydrodynamic ferromagnetic Sutterby fluid past a stretching curved surface. The effect of the chemical reaction, magnetic dipoles and thermal radiation are also considered. The x and y are used for curvilinear coordinates. The stretching surface is curled in a radius circle R'. Based on the linear velocity $u = Ax$ (A is constant), the surface is stretched in $x-$ direction and $y-$ direction while it is transverse to $x-$ direction. The surface is soaked in a non-Darcy porous medium. As the Reynolds number (magnetic) is smaller in the control problem, the electrical field and the induced magnetic field are ignored. Convective heat and mass transfer conditions are observed.

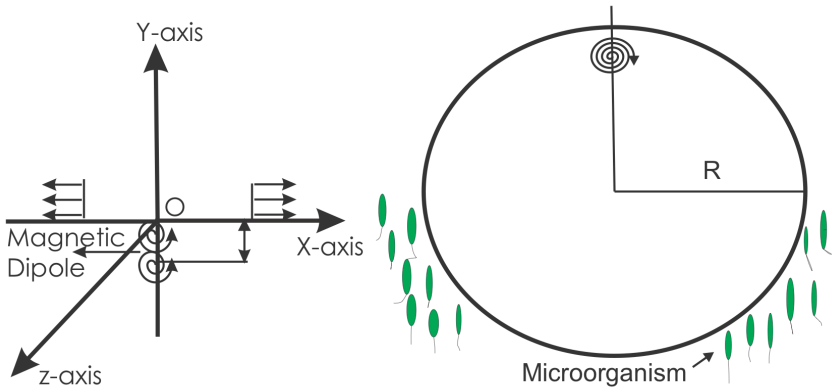

Figure 1. Geometry of the problem.

The boundary layer equations that govern the flow can be written in dimensional form under the above assumptions [10, 13, 20]

$$\frac{\partial\{(y+R')v\}}{\partial y} + R'\frac{\partial u}{\partial x} = 0, \tag{2.1}$$

$$\frac{u^2}{y+R'} = \frac{1}{\rho}\frac{\partial p}{\partial y} \tag{2.2}$$

$$\rho\left(v\frac{\partial u}{\partial y}+\frac{R'u}{y+R'}\frac{\partial u}{\partial x}+\frac{uv}{y+R'}\right)=u_e\frac{dU_e}{dx}\frac{R'}{y+R'}\frac{\partial p}{\partial x}$$
$$+\mu\left(\frac{\partial^2 u}{\partial y^2}-\frac{u}{(y+R')^2}+\frac{1}{y+R'}\frac{\partial u}{\partial y}\right)+\mu\frac{mE^2}{2}\left(\frac{\partial u}{\partial y}\right)^2\frac{\partial^2 u}{\partial y^2}$$
$$-\frac{\mu S_1}{k_o^*}u-\frac{\rho C_b S_1}{\sqrt{k_o^*}}u^2+\mu_o M\frac{\partial H}{\partial x}, \tag{2.3}$$

$$(\rho C_p)\left(\frac{R'u}{y+R'}\frac{\partial T}{\partial x}+v\frac{\partial T}{\partial y}\right)=\frac{k_T}{y+R'}\left[\frac{\partial T}{\partial y}+(y+R')\frac{\partial^2 T}{\partial y^2}\right]$$
$$+\left(u\frac{\partial H}{\partial x}+v\frac{\partial H}{\partial y}\right)\mu_o T\frac{\partial M}{\partial T}-\frac{k_T}{y+R'}\left(\frac{\partial q_r}{\partial y}(y+R')\right), \tag{2.4}$$

$$\frac{R'}{y+R'}u\frac{\partial C}{\partial x}+v\frac{\partial C}{\partial y}=\frac{D}{y+R'}\left(\frac{\partial C}{\partial y}+(y+R')\frac{\partial^2 C}{\partial y^2}\right)-K_c(C-C_\infty), \tag{2.5}$$

$$\left(\frac{R'}{y+R'}\right)u\frac{\partial N}{\partial x}+v\frac{\partial N}{\partial y}+\frac{bW_c}{C_w-C_\infty}\frac{\partial\left(N\frac{\partial C}{\partial y}\right)}{\partial y}=D_m\frac{\partial^2 N}{\partial y^2}, \tag{2.6}$$

with boundary conditions

$$u=Ax=U_w(x),\ \ v=0,\ -K\frac{\partial T}{\partial y}=h_1\big(T_w-T\big),$$
$$-D\frac{\partial C}{\partial y}=K_m\big(C_w-C\big),\ N=N_w\ at\quad y=0, \tag{2.7}$$

$$u\to 0,\quad \frac{\partial u}{\partial y}\to 0,\quad v\to 0,\quad T\to T_\infty,\ \ C\to C_\infty\quad N\to N_\infty,\quad as\quad y\to\infty, \tag{2.8}$$

where velocity components are (u,v) in the radial ($x-$ direction) and transverse ($y-$ direction), mass diffusion coefficient D_m, fluid density ρ, thermal conductivity k_T of fluid, electrical conductivity σ of fluid, dynamic viscosity μ, magnetic permeability μ_o, heat capacitance (ρc_p) of the fluid, first order chemical reaction parameter K_c, Microorganism diffusion coefficient D_n, gyrotactic Speed cell W_c, b chemotaxis, S_1 porosity of porous medium, T the temperature, C the concentration, N the gyrotactic Microorganism and T_∞, C_∞ and N_∞ stand for the temperature, concentration and density of microorganisms further away from the surface, respectively.

2.1. Magnetic Dipole

The characteristics of the magnetic field have an effect on the flow of ferrofluid due to the magnetic dipole. Magnetic dipole effects are recognized by the magnetic scalar potential Φ shown as in eq. (2.9)

$$\Phi=\frac{\gamma}{2\pi}\frac{x}{x^2+(y+c)^2} \tag{2.9}$$

With γ stands for magnetic field strength at the source. Taking H_x and H_y as the components of magnetic field as shown in Eqs. (2.10) and (2.11).

$$H_x=-\frac{\partial\Phi}{\partial x}=\frac{\gamma}{2\pi}\frac{x^2-(y+c)^2}{[x^2+(y+c)^2]^2} \tag{2.10}$$

$$H_y = -\frac{\partial \Phi}{\partial y} = \frac{\gamma}{2\pi}\frac{2x(y+c)}{[x^2+(y+c)^2]^2}. \tag{2.11}$$

Because of the magnetic body strength is usually proportional to the Hx and Hy gradient, it is therefore given as in (2.12)

$$H = \sqrt{H_x^2 + H_y^2}. \tag{2.12}$$

Eq. (2.13) can approximate the linear shape of magnetization M by temperature T

$$M = K_1(T - T_\infty), \tag{2.13}$$

The value of K_1 is identified as a ferromagnetic coefficient. Figure 1 shows the physical diagram of the ferrofluid.
Considering the following transformations [10]

$$u = Axf'(\zeta),\quad v = -\left(\frac{R'}{y+R'}\right)\sqrt{A\nu}f(\zeta),\quad p = \rho A^2x^2p(\zeta),\quad \zeta = y\sqrt{\frac{A}{\nu}},$$
$$\theta(\zeta) = \frac{T-T_\infty}{T_w-T_\infty},\quad \phi(\zeta) = \frac{C-C_\infty}{C_w-C_\infty},\quad \chi(\zeta) = \frac{N-N_\infty}{N_w-N_\infty}. \tag{2.14}$$

$$p' = \frac{f'^2}{\zeta+\alpha_1} \tag{2.15}$$

$$f''' + \frac{1}{\zeta+\alpha_1}f'' - \frac{1}{(\zeta+\alpha_1)^2}f' + \left(\frac{\alpha_1}{\zeta+\alpha_1}\right)\left[ff'' - f'^2 + \frac{1}{\alpha_1}f'f\right]$$
$$+ Def''f''' - P_1f' - L_if'^2 + \frac{2\beta}{(\zeta+d)^4}\theta + 2\left(\frac{\alpha_1}{\zeta+\alpha_1}\right)p = 0, \tag{2.16}$$

$$(1+Rd)\left(\theta'' + \frac{\theta'}{(\zeta+\alpha_1)}\right) + Pr\left(\frac{\alpha_1}{\zeta+\alpha_1}\right)f\theta' + \frac{2\beta\lambda(\theta-\epsilon)f}{(\zeta+d)^3}$$
$$+ \beta\lambda(\theta-\epsilon)\left[\frac{2f'}{(\zeta+d)^4} + \frac{4f}{(\zeta+d)^5}\right] = 0, \tag{2.17}$$

$$\phi'' + \frac{\phi'}{(\zeta+\alpha_1)} + \left(\frac{\alpha_1}{\zeta+\alpha_1}\right)Scf\phi' - \delta Sc\phi = 0, \tag{2.18}$$

$$\chi'' + Pe[\phi'\chi' + \phi''\chi + N_\delta\phi''] + Le\left(\frac{\alpha_1}{\zeta+\alpha_1}\right)f\chi' = 0. \tag{2.19}$$

To eliminate the pressure term from integrate (2.15) to get p and replace it, then (2.16) becomes

$$f''' + \frac{1}{\zeta+\alpha_1}f'' - \frac{1}{(\zeta+\alpha_1)^2}f' + \left(\frac{\alpha_1}{\zeta+\alpha_1}\right)\left[ff'' - f'^2 + \frac{1}{\alpha_1}f'f\right]$$
$$+ Def''f''' - P_1f' - L_if'^2 + \frac{2\beta}{(\zeta+d)^4}\theta + \left(\frac{\alpha_1}{(\zeta+\alpha_1)^2}\right)(2ff'' - f'^2) = 0, \tag{2.20}$$

with boundary conditions

$$f'(0) = 1, f(0) = 0, f(\infty) = 0, f''(\infty) = 0,\ \theta'(0) = -B_{i1}[1-\theta(0)], \theta(\infty) = 0,$$
$$\phi'(0) = -B_{i2}[1-\phi(0)], \phi(\infty) = 0, \chi'(0) = 1, \chi(\infty) = 0, \tag{2.21}$$

where α_1 is the curvature parameter, d dimensionless distance, β is the ferrohydrodynamic interaction, λ is heat dissipation parameter, ε is the curie temperature, Pr is Prandtl number, Rd is thermal radiation parameter, D and D_m the ratio of the diffusion coefficients, δ is the chemical reaction parameter, Sc is the Schmidt number, De is Deborah number, Li is the local inertia parameter, P_1 is the porosity parameter, B_{i1} is thermal Biot number and B_{i2} is concentration Biot number, Pe is Peclet number, Le is the Lewis number, are dimensionless quantities given by

$$\begin{aligned}
&\alpha_1 = R'\sqrt{\frac{A}{\nu}}, p_1 = \frac{\mu S_1}{\rho A k_o^*}, L_i = \frac{C_b S_1}{\sqrt{k_o^*}}, \beta = \frac{\gamma \mu_o K_1 \rho (T_w - T_\infty)}{2\pi\mu^2}, Pr = \frac{\mu C_p}{k_T},\\
&\lambda = \frac{A\mu^2}{\rho(T_w - T_\infty)k_T}, d = \sqrt{\frac{Ac^2}{\nu}}, B_{i1} = \frac{h_1}{k_T}\sqrt{\frac{\nu}{A}}, B_{i2} = \frac{K_m}{k_T}\sqrt{\frac{\nu}{A}},\\
&De = \frac{mE^2(Ax)^2}{\nu}, Rd = \frac{16\sigma^* T_\infty^3}{3kk^*}, Pe = \frac{bW_c}{D_n}, Le = \frac{\nu}{D_n}, , N_\delta = \frac{N_\infty}{N_w - N_\infty},\\
&\delta = \frac{AK_c}{\nu} Sc = \frac{\nu}{D_m}, Re = \frac{A}{\nu}, \epsilon = \frac{T_\infty}{T_\infty - T_w}.
\end{aligned} \tag{2.22}$$

The interesting physical quantities, including skin friction, local Nusselt, Sherwood numbers and local density numbers, are determined accordingly by

$$\begin{aligned}
&C_f = \frac{\tau_{yx}}{\rho(Ax)^2}, \ Nu_x = \frac{-xq_w}{k_T(T_w - T_\infty)},\\
&Sh_x = \frac{-xq_m}{D(C_w - C_\infty)} \ Sn_x = \frac{-xq_n}{D_m(N_w - N_\infty)}
\end{aligned} \tag{2.23}$$

$$\tau_{yx} = \mu u_y|_{y=0}, \ q_w = -k^* T_y|_{y=0}, \ q_m = -DC_y|_{y=0} \ q_n = D_m N_y|_{y=0} \tag{2.24}$$

$$\begin{aligned}
&C_f = \frac{1}{Re_x}\left(f''(0) - \frac{Def'(0)}{\alpha_1}\right), \ Nu = -Re_x^{0.5}(1 + Rd)\theta'(0),\\
&Sh = -Re_x^{0.5}\phi_1'(0), \ Sn = -Re_x^{0.5}\chi'(0)
\end{aligned} \tag{2.25}$$

3. HAM Solutions methodology

Taking the initial guesses and the linear operators as

$$f_0(\zeta) = (1 - e^{-\zeta}), \ \theta_0(\zeta) + \frac{B_{i1}}{1 + B_{i1}} e^{-\zeta}, \ \phi_0(\zeta) = \frac{B_{i2}}{1 + B_{i2}} e^{-\zeta}, \ \chi_0 = e^{-\zeta}. \tag{3.1}$$

equation (3.1) satisfy the properties given below

$$\begin{aligned}
&L_f(Q_1 + Q_2 e^{\zeta} + Q_3 e^{-\zeta}) = 0, \ \ L_\theta(Q_4 e^{\zeta} + Q_5 e^{-\zeta}) = 0,\\
&L_\phi(Q_6 e^{\zeta} + Q_7 e^{-\zeta}) = 0, \ \ L_\chi(Q_8 e^{\zeta} + Q_9 e^{-\zeta}) = 0
\end{aligned} \tag{3.2}$$

where $Q_i (i = 1, ..., 9,)$ indicates the arbitrary constants.

4. Result and Discussion

4.1. Velocity Profile

Figure 2 depicts the effect of α_1 on the velocity profile. The figure shows that the velocity of the fluid increases by α_1. Figure 3 shows the performance of the ferromagnetic hydrodynamic interaction parameter β in the velocity profile. The velocity behavior is decelerating by β. Usually, the resistance force classified as Lorentz force increases with β and the velocity decreases. Figure 4 shows the velocity behavior of the Deborah number De. this number is used to illuminate the viscoelasticity characteristics of the Sutterby material. By increase the De the flow velocity of Sutterby fluid increases. Higher fluid motion increases the thickness of the hydrodynamic boundary layer and therefore increases the velocity of the fluid. Figure 5 depicts the effect of porosity parameter P_1. The present porous medium slows down the flow field, resulting in an increase in shear stress on the curved surface and, as a result, the velocity profile shows a declining trend by increasing the values of P_1.

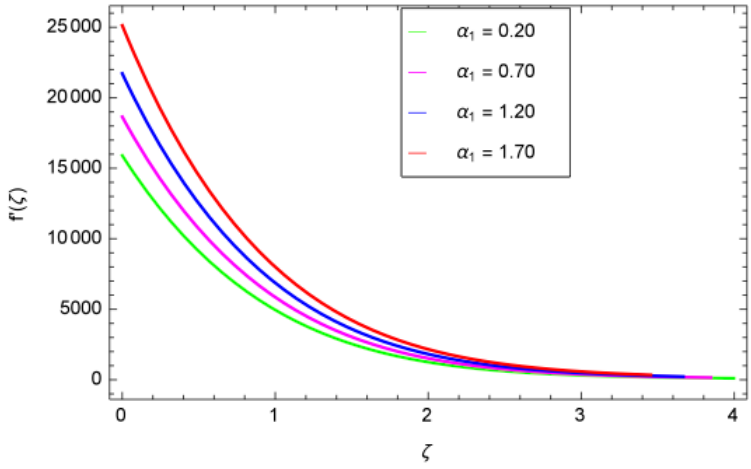

Figure 2. $f'(\zeta)$ as a function of α_1.

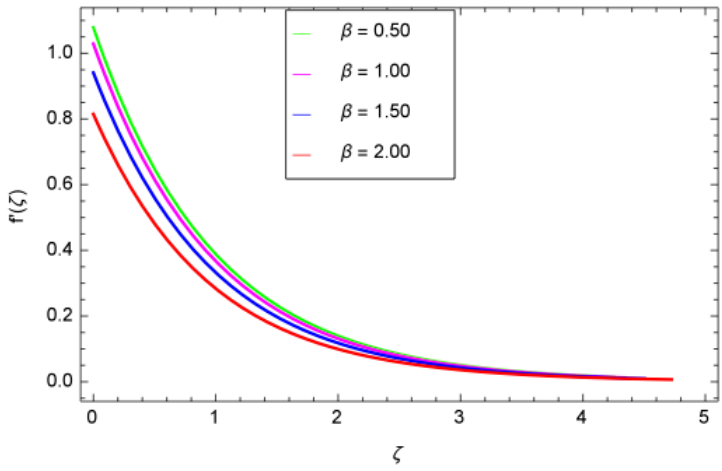

FIGURE 3. $f'(\zeta)$ as a function of β.

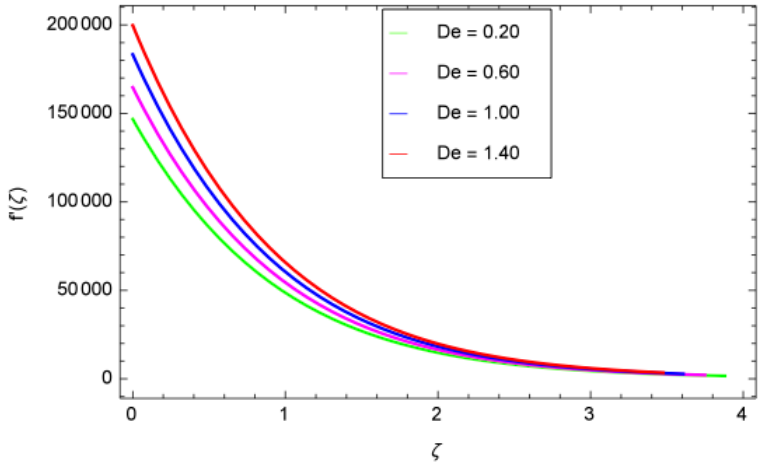

FIGURE 4. $f'(\zeta)$ as a function of De.

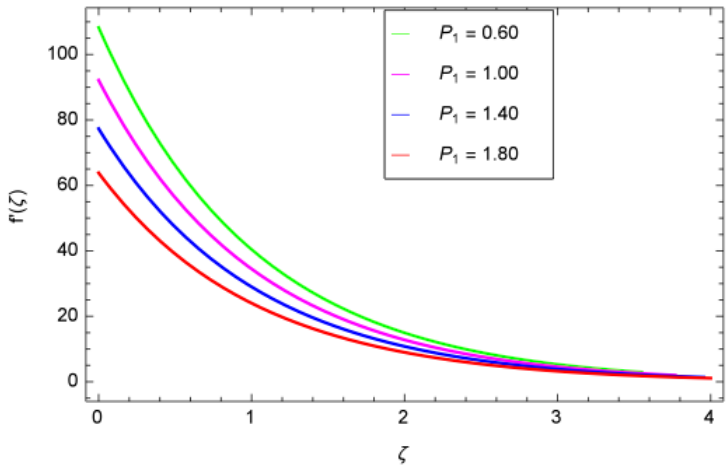

FIGURE 5. $f'(\zeta)$ as a function of P_1.

4.2. Temperature Profile

Figure 6 depicts the effect of α_1 on the velocity profile. In the figure the velocity component increases with the increase in α_1 value. Figure 7 illustrated the effects of β on temperature. The temperature of the fluid increases with the increase in β.Figure 8 shows that, the temperature decreases by increasing of ε. Fluid thermal conductivity increases with the larger ε. As a result, the extra heat is transfered from the surface to the fluid material and the temperature increases. Figure 9 shows the effect of λ on temperature. The temperature decreases with an increase in λ. Physically thermal conductivity of fluid decay with larger λ, hence the temperature reduces. Figure 10 depicts the impact of Bi_1 on temperature profile. It is observed that the temperature is rising by Bi_1. Bi_1 depends on the coefficient of heat transfer or, in other words, is directly proportional to the coefficient of heat transfer (which is greater for Bi_1). Figure 11 shows the temperature response for Prandtl number Pr. The temperature of the Sutterby fluid decreases with the higher Pr. Physically, Prandtl number refers to thermal diffusivity. Larger Pr is the lower thermal diffusivity which causes the temperature to decomposed. Figure 12 shows that the temperature of the fluid increases due to the increase in the radiation parameter Rd. In this case, the absorption coefficient decreases with an increase in Rd, which leads to an increase in the rate of radiative heat transfer.

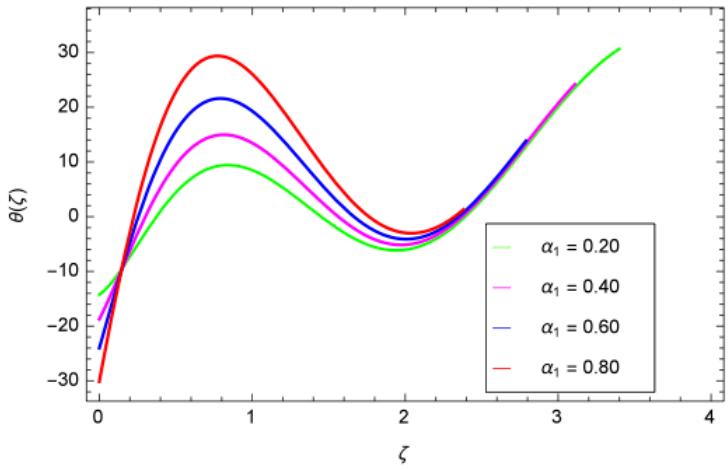

FIGURE 6. $\theta(\zeta)$ as a function of α_1.

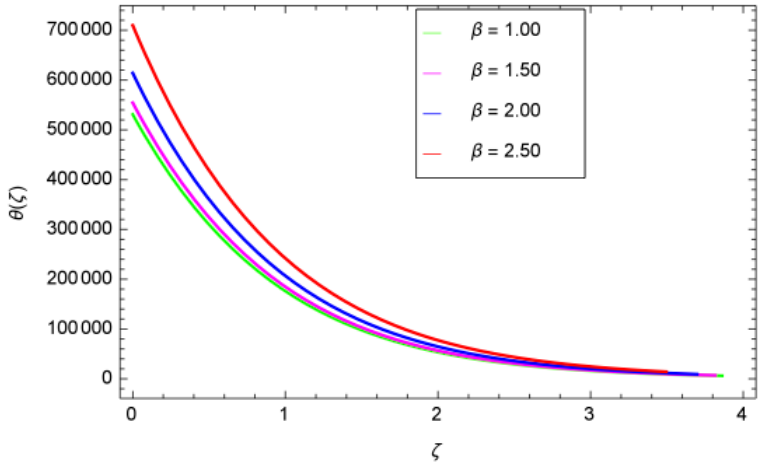

FIGURE 7. $\theta(\zeta)$ as a function of β.

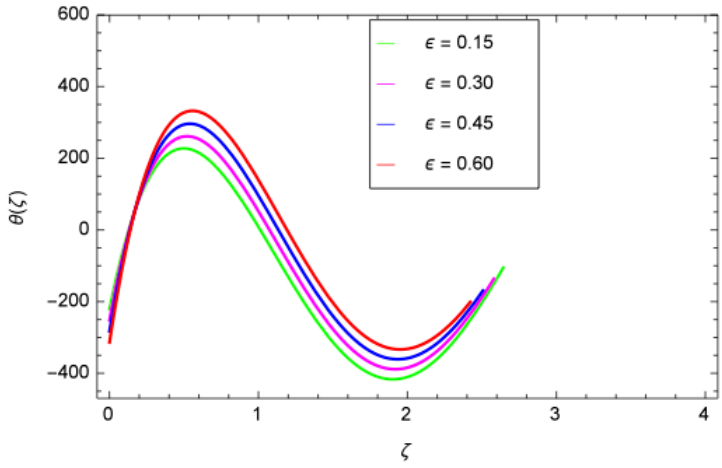

FIGURE 8. $\theta(\zeta)$ as a function of ε.

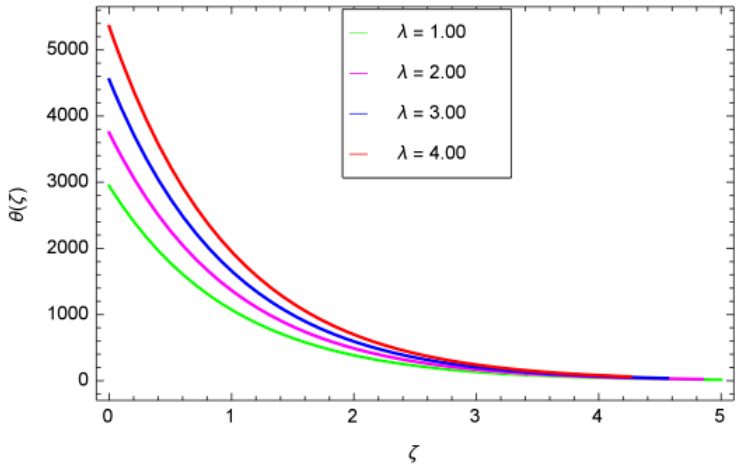

FIGURE 9. $f'(\zeta)$ as a function of λ.

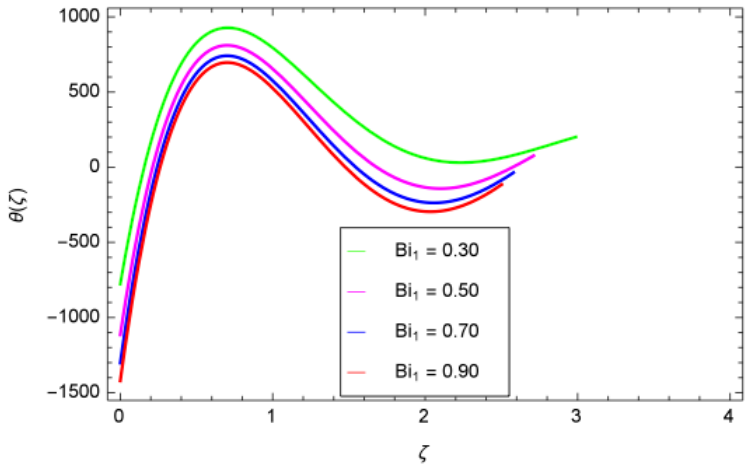

FIGURE 10. $\theta(\zeta)$ as a function of Bi_1.

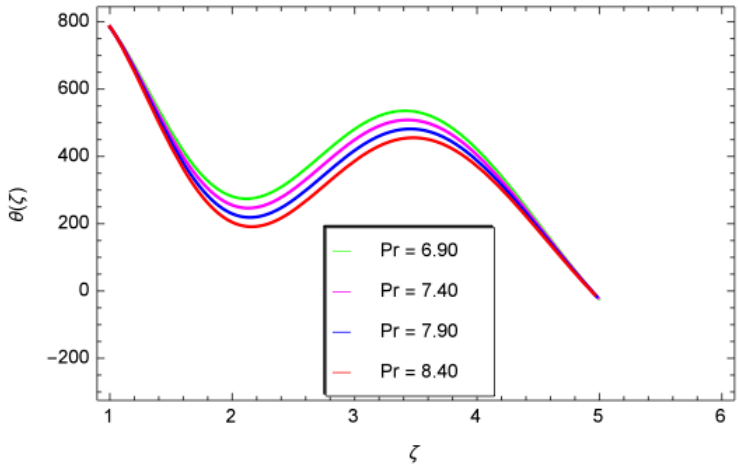

FIGURE 11. $\theta(\zeta)$ as a function of Pr.

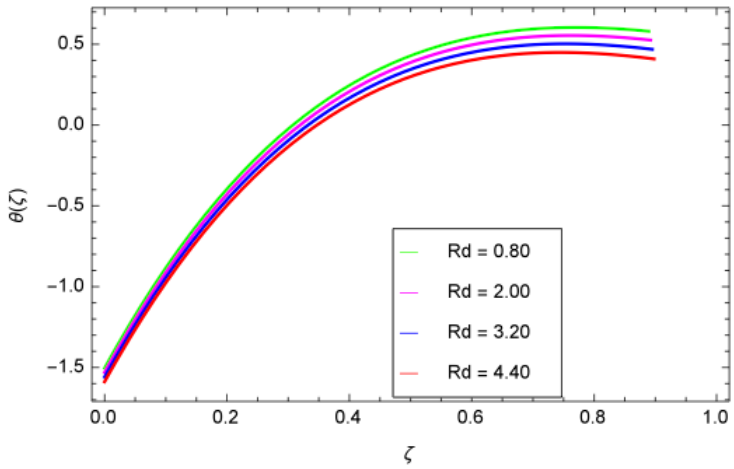

FIGURE 12. $\theta(\zeta)$ as a function of Rd.

4.3. Concentration Profile

Figure 13 depicts the impact of the chemical reaction parameter δ. It is observed the concentration of fluid decreased by δ. Figure 14 shows the effect of Schmidt number Sc on the concentration profile. The concentration of the particles increased by an increasing the Schmidt number.

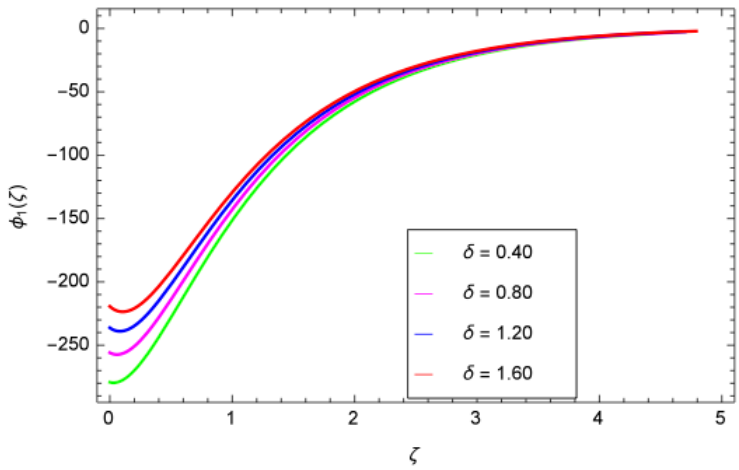

FIGURE 13. $\phi(\zeta)$ as a function of δ.

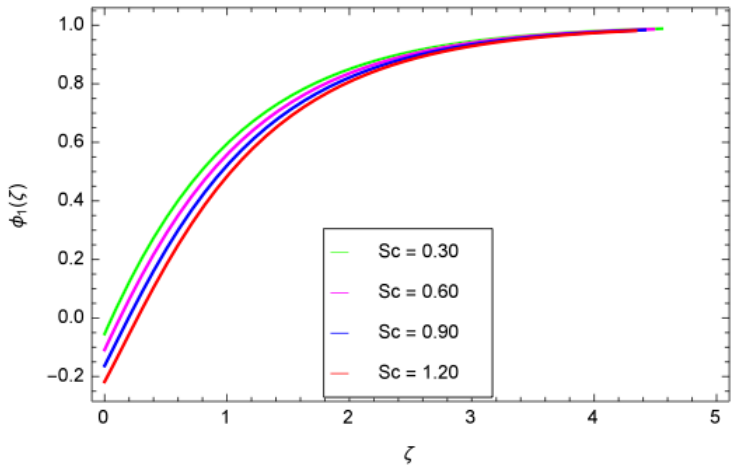

FIGURE 14. $\phi(\zeta)$ as a function of Sc.

4.4. MICROOGANISM MOTILE PROFILE

Figure 15 shows the effect of Peclet number Pe on the profile of the motile microorganism. There is a clear connection between the improved density of the motile microorganism with the increasing values of Pe. Figure 16 shows the effect of Lewis number Le on the motile microorganism profile. The reduction in the concentration distribution could be seen as the Lewis number was inversely proportional to the mass diffusion.

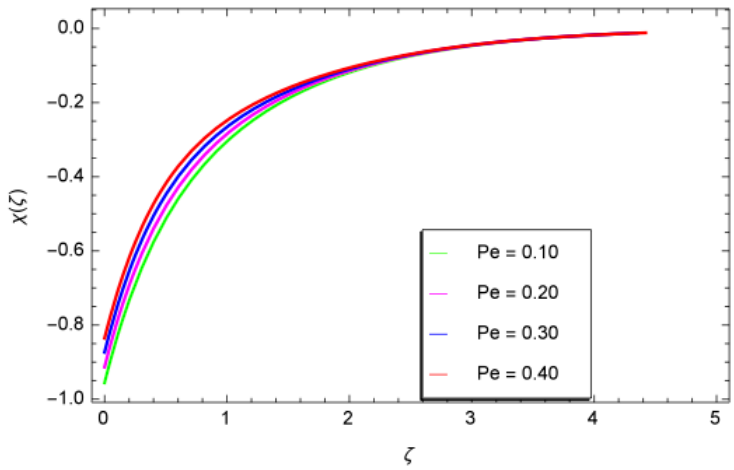

FIGURE 15. $\chi(\zeta)$ as a function of Pe.

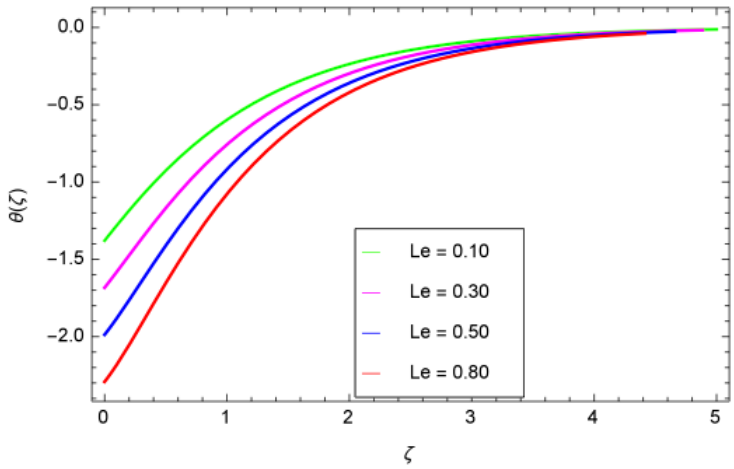

FIGURE 16. $\phi(\zeta)$ as a function of Le.

4.5. NUMERICAL VALUES OF NUSSELT, SHEWOOD AND LOCAL DENSITY NUMBERS

Table 1 depicts the numerical estimation of the local Nusselt number for various values of $\beta, \alpha_1, \lambda, Pr, Rd, \varepsilon, Bi_1$. It is observed that the local Nusselt number decreases with increasing values of $\beta, \alpha_1, \lambda, Bi_1$.Table 2 depicts the numerical values of the local Sherwood number for various values of α_1, Sc, δ. It is observed that the local Sherwood number decreases with the increasing values of all the three parameters. Table 3 shows the numerical values of the local density number for various values of $\alpha_1, Pe, Le, N_\delta$. It is observed that the local density number decreases with the increasing values of all the parameters except N_δ. The tables clearly show that the current findings are completely consistent.

TABLE 1. Numerical values of Nusselt number with varying values of the parameters $\beta, \alpha_1, \lambda, Pr, Rd, \varepsilon, Bi_1$.

$\boldsymbol{\beta}$	$\boldsymbol{\varepsilon}$	$\boldsymbol{\lambda}$	$\boldsymbol{\alpha_1}$	$\boldsymbol{Rd}$	$\boldsymbol{Bi_1}$	$\boldsymbol{\theta'(0)}$
0.4	0.3	0.2	0.5	0.4	0.2	0.34701
0.8						0.35167
1.2						0.36752
	0.4					0.39766
	0.5					0.38914
	0.6					0.37245
		0.5				0.35806
		0.8				0.35739
		1.1				0.35623
			1.5			0.73123
			2.5			0.67433
			3.5			0.54876
				0.5		0.43342
				0.6		0.42534
				0.7		0.41998
					0.4	0.61291
					0.6	0.63854
					0.8	0.64554

TABLE 2. Numerical values of Sherwood number with varying values of the parameters α_1, Sc, δ.

$\boldsymbol{\delta}$	**Sc**	$\boldsymbol{\alpha_1}$	$\boldsymbol{\phi'(0)}$
0.1	0.3	0.2	0.54237
0.3			0.53831
0.5			0.52633
	0.5		0.61271
	0.7		0.62220
	0.9		0.63742
		0.4	0.67472
		0.6	0.61386
		0.8	0.56075

Table 3. Numerical values of local density number with varying values of the parameters N_δ, Pe, Le, α_1.

N_δ	Pe	Le	α_1	$\chi'(0)$
0.1	0.3	0.2	0.2	0.25238
0.2				0.26103
0.3				0.27271
	0.4			0.39327
	0.5			0.35102
	0.6			0.32714
		0.3		0.26671
		0.4		0.22386
		0.5		0.23185
			0.3	0.35408
			0.4	0.34965
			0.5	0.34121

5. Conclusion

The Darcy-Forchheimer model of hydromagnetic flow of Sutterby ferrofluid on a curved stretching surface with chemical reaction, thermal radiation, and the presence of magnetic dipoles effect was investigated. Through similarity transformations, the resulting non-dimensional ordinary differential equations were obtained, and the results were numerically presented. The main points are as follows:

- The velocity has declined with the increasing ferro-hydrodynamic interaction parameter and porosity parameter and increases with the curvature parameter, Debora number and heat dissipation parameter.
- Temperature increases with an increasing value of curvature parameter, ferro-hydrodynamic interaction parameter and thermal radiation parameter, and decreases with Prandtl number.
- Larger chemical reaction parameter portrays a rising in the concentration, while Schmidt number lead to the reduction in concentration.
- The motile density of microorganism increases with Peclet number and decreases with Lewis number.

References

[1] J.L. Sutterby, Laminar converging flow of dilute polymer solutions in conical sections: Part I. Viscosity data, new viscosity model, tube flow solution, AIChE Journal 12 (1) (1966) 63–8.

[2] J.L. Sutterby, Laminar converging flow of dilute polymer solutions in conical sections II, Transactions of the Society of Rheology 9 (2) (1965) 227–41.

[3] R.L. Batra, M. Eissa, Helical flow of a Sutterby model fluid, Polymer-Plastics Technology and Engineering 33 (4) (1994) 489–501.

[4] M.M. Fayyadh, K. Naganthran. M.F. Basir, I. Hashim, R. Roslan, Radiative MHD Sutterby Nanofluid Flow Past a Moving Sheet: Scaling Group Analysis, Mathematics 8 (9) (2020) 430.

[5] T. Hayat, S. Ayub, A. Alsaedi, A. Tanveer, B. Ahmad, Numerical simulation for peristaltic activity of Sutterby fluid with modified Darcys law, Results in physics 7 (2017) 762–8.
[6] M.A. Mir, M. Farooq, M. Rizwan, F. Ahmad, S. Ahmad, B. Ahmad, Analysis of thermally stratified flow of Sutterby nanofluid with zero mass flux condition, Journal of Materials Research and Technology 9 (2) (2020) 1631–1639.
[7] P. Forchheimer, Wasserbewegung durch boden, Z. Ver. Deutsch, Ing. 45 (1901) 1782–1788.
[8] D.A. Nield, A. Bejan, Convection in porous media, springer, New York, 2006.
[9] N. Kishan, S. Maripala, Thermophoresis and viscous dissipation effects on Darcy-Forchheimer MHD mixed convection in a fluid saturated porous media, Advances in applied science Research 3 (2012) 60–74.
[10] A. Rauf, Z. Abbas, S.A. Shehzad, T. Mushtaq, Thermally Radiative Viscous Fluid Flow Over Curved Moving Surface in Darcy-Forchheimer Porous Space, Communications in Theoretical Physics 71 (2019) 259.
[11] S. Jagadha, P. Amrutha, MHD Boundary Layer Flow of Darcy-Forchheimer Mixed Convection in a Nanofluid Saturated Porous Media with Viscous Dissipation, International Journal of Applications and Applied Mathematics, AAM Special Issue 4 (2019) 117–34.
[12] H.I. Andersson, O.A. Valnes, Flow of a heated ferrofluid over a stretching sheet in the presence of a magnetic dipole, Acta Mechanica 128 (1998) 39–47.
[13] T. Hayat, S. Ahmad, M.I. Khan, A. Alsaedi, Exploring magnetic dipole contribution on radiative flow of ferromagnetic Williamson fluid, Results in physics 8 (2018) 545–551.
[14] L.R. Titus, A. Abraham, Heat transfer in ferrofluid flow over a stretching sheet with radiation, Int. J. Eng. Res. Tech. 3 (2014) 2198–203.
[15] G.H. Kefayati, Natural convection of ferrofluid in a linearly heated cavity utilizing LBM. *Journal of Molecular Liquids* 191 (2014) 1–9.
[16] S. Afkhami, Y. Renardy, Ferrofluids and magnetically guided superparamagnetic particles in flows: a review of simulations and modeling, Journal of Engineering Mathematics 107 (2017) 231–51.
[17] W.R. Williams, M.T. Stenzel, X. Song, Schmidt LD. Bifurcation behavior in homogeneous-heterogeneous combustion: I. Experimental results over platinum, Combustion and flame 84 (3-4) (1991) 277–91.
[18] W.R. Williams, J. Zhao, Schmidt LD. Ignition and extinction of surface and homogeneous oxidation of NH3 and CH4, AIChE journal 37 (5) (1991) 641–649.
[19] B.C. Sakiadis, Boundary-layer behavior on continuous solid surfaces: I. Boundary-layer equations for two-dimensional and axisymmetric flow, AIChE Journal 7 (1) (1961) 26–28.
[20] R. Muhammad, M.I. Khan, M. Jameel, K.B. Khan, Fully developed Darcy-Forchheimer mixed convective flow over a curved surface with activation energy and entropy generation. *Computer Methods and Programs in Biomedicine* 188 (2020) 105298.
[21] S. Ahmad, S. Nadeem, N. Muhammad. Boundary layer flow over a curved surface imbedded in porous medium, Communications in Theoretical Physics 71 (3) (2019) 344.

[22] W.A. Khan, M. Waqas, M. Ali, F. Sultan, M. Shahzad, M. Irfan, Mathematical analysis of thermally radiative time dependent Sisko nanofluid flow for curved surface, International Journal of Numerical Methods for Heat and Fluid Flow (2019).
[23] S.J. Liao, An explicit, totally analytic approximate solution for Blasius viscous flow problems, International Journal of Non-Linear Mechanics 34 (1999) 759–78.
[24] S.J. Liao, Beyond perturbation: introduction to the homotopy analysis method, CRC press, 2003.
[25] S.J. Liao, Homotopy analysis method in nonlinear differential equations, Higher Education Press Beijing and Springer-Verlag Berlin Heidelberg, 2012.
[26] N.S. Khan, Bioconvection in second grade nanofluid flow containing nanoparticles and gyrotactic microorganisms, Brazilian Journal of Physics 48 (2018) 227–241.
[27] Z. Shah, S. Islam, T. Gul, E. Bonyah, M.A. Khan, The electrical MHD and hall current impact on micropolar nanofluid flow between rotating parallel plates, Results in physics 9 (2018) 1201–1214.
[28] A.H. Usman, N.S. Khan, U.W. Humphries, Z. Ullah, Q. Shah, P. Kumam, P. Thounthong, W. Khan, A. Kaewkhao, A. Bhaumik, Computational optimization for the deposition of bioconvection thin Oldroyd-B nanofluid with entropy generation, Scientific reports 11 (1) (2021) 1–23.
[29] A.H. Usman, N.S. Khan, U.W. Humphries, Z. Shah, P. Kumam, W. Khan, A. Khan, S.A. Rano, Z. Ullah, Development of dynamic model and analytical analysis for the diffusion of different species in non-Newtonian nanofluid swirling flow. Front. Phys. 8 (2021) 616790.
[30] N.S. Khan, A.H. Usman, A. Sohail, A. Hussanan, Q. Shah, N. Ullah, P. Kumam, P. Thounthong, A Framework for the Magnetic Dipole Effect on the Thixotropic Nanofluid Flow Past a Continuous Curved Stretched Surface, Crystals 11 (6) (2021) 645.